

THE EVENT HORIZON OF SAGITTARIUS A*

AVERY E. BRODERICK¹, ABRAHAM LOEB² & RAMESH NARAYAN²

Draft version September 11, 2018

ABSTRACT

Black hole event horizons, causally separating the external universe from compact regions of space-time, are one of the most exotic predictions of General Relativity (GR). Until recently, their compact size has prevented efforts to study them directly. Here we show that recent millimeter and infrared observations of Sagittarius A* (Sgr A*), the supermassive black hole at the center of the Milky Way, all but requires the existence of a horizon. Specifically, we show that these observations limit the luminosity of any putative visible compact emitting region to below 0.4% of Sgr A*'s accretion luminosity. Equivalently, this requires the efficiency of converting the gravitational binding energy liberated during accretion into radiation and kinetic outflows to be greater than 99.6%, considerably larger than those implicated in Sgr A*, and therefore inconsistent with the existence of such a visible region. Finally, since we are able to frame this argument entirely in terms of observable quantities, our results apply to all geometric theories of gravity that admit stationary solutions, including the commonly discussed $f(R)$ class of theories.

Subject headings: black hole physics — Galaxy: center — techniques: interferometric — infrared: general

1. INTRODUCTION

The Schwarzschild metric presents the first example of a compact horizon: an imaginary surface delineating a compact region from which the rest of the universe is causally disconnected. Subsequently, a substantial theoretical effort was made to determine if such “black hole” solutions could practically come into existence (Oppenheimer & Snyder 1939; Penrose 1965; Wheeler 1966; Heger et al. 2003). Despite Einstein’s misgivings, black holes are now believed to be the inevitable consequence of the demise of massive stars. In recent years, the existence of compact horizons has taken on a renewed significance due to efforts to construct a Grand Unified Theory. Specifically, horizons play prominently in the well known “information paradox” (Hawking 2005; Mathur 2007). However, now we are in a position to constrain the existence of horizons observationally.

For astrophysical purposes, the critical features of horizons are (1) their compactness, allowing substantial amounts of gravitational binding energy to be liberated during accretion, and (2) their ability to hide the ultimate fate of accreting matter. Unlike a black hole, into which the kinetic and thermal energy gained during infall can disappear (adding only to the mass), objects with surfaces (e.g., stars) radiate the residual energy not emitted during the accretion process. This fact has been used in a number of efforts to test for the presence of horizons in a variety of black hole systems (Narayan et al. 1997; Narayan & Heyl 2002; McClintock et al. 2004; Broderick & Narayan 2006, 2007; Narayan & McClintock 2008). For many black hole candidates the tell-tale sign of surface emission, seen in accreting neutron stars, is absent, implying the lack of an analogous surface in these objects.

Sagittarius A* (Sgr A*), the radio point-source associated with the dark mass located at the center of the Milky Way, is the best studied black hole candidate to date. Near-infrared (NIR) observations of massive stars in its vicinity have provided direct mass and distance measurements, $M = 4.5 \pm 0.4 \times 10^6 M_{\odot}$ and $D = 8.4 \pm 0.4$ kpc, respectively, and confined it to within 40 AU (Ghez et al. 2008; Gillessen et al. 2008). With a luminosity of 10^{36} ergs⁻¹, it is substantially underluminous relative to its limiting Eddington luminosity, 6×10^{44} ergs⁻¹. The emission is strongly non-thermal, distributed from the radio to γ -rays, and believed to be powered by the release of gravitational binding energy by accreting gas.

Due to its mass and proximity, Sgr A* has the largest angular size of any known black hole and offers the best prospects for direct imaging of its silhouette (Falcke et al. 2000; Broderick & Loeb 2005, 2006a,b). Unfortunately, mm-imaging alone will be unable to verify or exclude the presence of a horizon (Broderick & Narayan 2006). This is because even a relatively bright central object (e.g., one radiating thermally with a luminosity comparable to $\dot{M}c^2$) will appear in silhouette against the much hotter surrounding accretion flow. However, here we show that recent mm-Very Long Baseline Interferometric (VLBI) observations, which have resolved sub-horizon scale structure for the first time (Doeleman et al. 2008), provide conclusive evidence for the presence of a horizon when coupled with the existing NIR and mid-infrared (MIR) flux limits (Ghez et al. 2005; Hornstein et al. 2007; Schödel et al. 2007). We do this by explicitly excluding emission from a putative compact infrared photosphere, lying inside of the mm-emitting region. Specifically, we show that for such surface emission to remain undetected would require unphysically large radiative efficiencies; greater than 99.6%, as compared to the typical efficiencies in AGN of 10% (Kato et al. 2008) and the meager efficiency implicated in Sgr A*, 0.01–1% (Narayan & McClintock 2008). Most importantly, we do

¹ Canadian Institute for Theoretical Astrophysics, 60 St. George St., Toronto, ON M5S 3H8, Canada; aeb@cita.utoronto.ca

² Institute for Theory and Computation, Harvard University, Center for Astrophysics, 60 Garden St., Cambridge, MA 02138.

this using only observable quantities, ensuring that these limits are largely independent of the gravitational theory employed³.

§2 describes the underlying physical assumptions and §3 presents the recent observational constraints, within the context of Sgr A*. Conclusions are collected in §4. Appendices A and B discuss photon propagation times, the notion of gravitational binding energy and the apparent size of objects within the context of general geometric theories of gravity.

2. PHYSICAL ASSUMPTIONS

Our argument depends critically upon three underlying, physically well motivated assumptions: (1) Sgr A* is accretion powered, (2) has reached steady state and (3) compact surfaces are approximate blackbodies. We wish to emphasize that relaxing any of these would require fundamental alterations to presently well understood physics (such as microscopic physics at pedestrian, and laboratory accessible, densities, temperatures and magnetic field strengths). Nevertheless, we discuss each in detail, describing how these are justified in the context of Sgr A*.

2.1. Accretion Power & the Luminosity of Sgr A*

It has been widely accepted that the emission from Sgr A* is powered by accretion. This is inferred from a variety of sources, including the spectrum, variability, VLBI observations, environment and polarization of Sgr A*. Here we review these, if only to list the numerous observational hurdles facing any alternate interpretation.

The spectrum of Sgr A* extends from the radio to the gamma-rays, peaking in the sub-mm, where it transitions from a featureless, inverted power-law to an optically thin spectrum. Sgr A*'s emission is strongly non-thermal and exhibits no absorption lines, which despite its low bolometric luminosity (comparable to a B-star) rules out a hydrostatic, optically thick gas cloud, similar to a large star. Furthermore, this spectrum is very similar to that from other AGN, for which there is no known alternative power source with the necessary efficiency.

At cm-wavelengths and below, Sgr A* exhibits considerable short timescale variability. Flares have been observed in the mm, sub-mm, infrared and X-ray bands, with rise times and variability timescales comparable to the periods of innermost stable orbits around General Relativistic (GR) black holes. At considerably longer wavelengths, where Sgr A* is optically thick, the degree of variability decreases and the characteristic timescales increase. This is consistent with a stratified emitting region, with short-wavelength emission arising close to the central mass.

This interpretation is confirmed by VLBI observations. Observations with the Very Long Baseline Array at wavelengths from 3 mm to 6 cm have resolved the intrinsic size of the radio emitting region about Sgr A* (Bower et al. 2006; Shen et al. 2005; Krichbaum et al. 2006). This is somewhat complicated by interstellar scattering, requiring a careful subtraction of the scattering law determined

by fitting the observed size of Sgr A* from 6 cm to 24 cm. While there is some debate over the precise form of the scattering law, there is no question that Sgr A* is indeed radially stratified, with the radius of the photosphere decreasing with decreasing wavelength.

Turning to its environment, Sgr A* suffers from an embarrassment of riches. The stellar winds from nearby massive stars ($\simeq 0.1$ pc from Sgr A*) provide sufficient material to support luminosities more than 11 orders of magnitude greater than that observed! Indeed, the difficulty in modeling Sgr A* has been to explain its meager luminosity instead of the prodigious output predicted. This has typically been done by postulating an extraordinarily low radiative efficiency and/or the existence of accretion-powered outflows (Narayan et al. 1995; Blandford & Begelman 1999).

Finally, below roughly 3 mm, Sgr A* is linearly polarized (Aitken et al. 2000; Bower et al. 2003; Macquart et al. 2006; Marrone et al. 2006, 2007). At longer wavelengths it is Faraday depolarized, providing some measurement of the density and magnetic field strength near the central mass. Assuming near equipartition magnetic fields, this implies a density of cold electrons of roughly 10^6 cm^{-3} at radii of 10^{13-14} cm (Agol 2000; Quataert & Gruzinov 2000; Marrone et al. 2006). Assuming stronger, large-scale magnetic fields results in lower density estimates, and conversely, large amounts of magnetic turbulence results in higher estimates. While this does not provide a direct measurement of the accretion rate, it is difficult to imagine that the magnetorotational instability is incapable of driving accretion in this environment at rates up to $10^{-8} \dot{M}_{\odot}/\text{yr}$.

2.2. Steady State

Assuming steady state will allow us to relate the surface emission from black hole alternatives to that from the accretion flow. Within the context of Sgr A* there are a variety of reasons to expect that any black hole alternative will have reached some sort of steady state (see Broderick & Narayan 2007). However, we point out that black holes explicitly violate this condition: the unradiated kinetic energy is advected across the horizon and then added to the mass of the black hole.

The dynamical timescale of Sgr A* depends upon the nature of the object. Nevertheless, we may expect that it is comparable to the dynamical timescale of the corresponding black hole, $GM/c^3 \simeq 20$ s. This is supported by the ~ 10 min variability observed in the NIR and X-rays, presumed to be associated with material orbiting nearby. Both of these are much, much shorter than the estimated age of Sgr A*, 10 Gyr, making it natural to assume that it has sufficient time to reach steady state. Note that if a substantial portion of Sgr A*'s mass was accrued via accretion, its accretion rate must have been much larger at times in the past. Thus if the timescale for reaching steady state exceeds the period since the previous active phase we will be *underestimating* Sgr A*'s luminosity.

While the extreme difference in timescales naturally implies that even surfaces with extraordinary redshifts ($z \lesssim 10^{15}$) will have reached steady state, within the context of black hole alternatives exhibiting GR exterior spacetimes a much stronger statement can be made. This is because photons that are emitted initially outward and subsequently lensed back onto Sgr A* necessarily pro-

³ Our results hold for any geometric gravitational theory admitting stationary solutions. This includes all of the $f(R)$ theories as well as black hole alternatives within the context of General Relativity, such as clusters of compact objects, boson stars and gravastars.

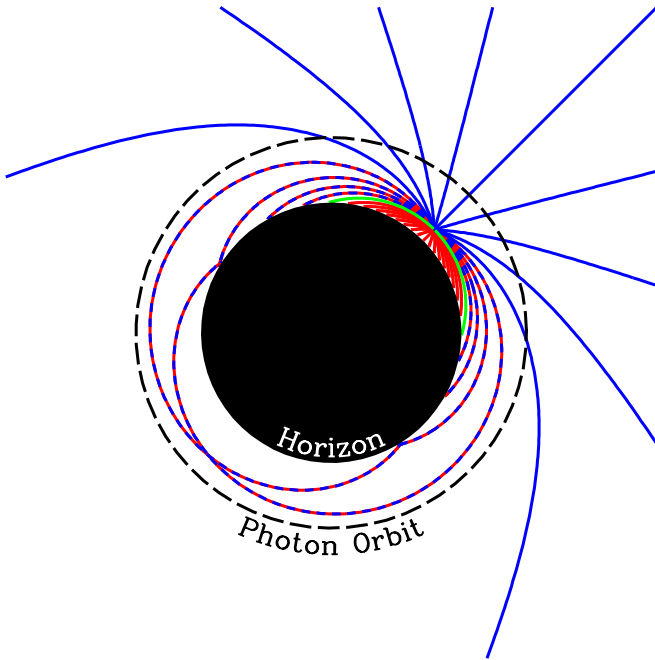


FIG. 1.— Rays launched isotropically (every 10°) in the locally flat, stationary frame are lensed in a Schwarzschild spacetime. Those rays that are initially moving inwards, tangentially and outwards are shown in red, green and blue, respectively. Additionally, those that are launched initially moving outwards and are subsequently captured are red-blue dashed. For reference the horizon and photon orbit are shown. Generically, the fraction of rays that escape to infinity decreases as the emission point is moved towards the black hole, dropping below 50% at the photon orbit and dropping all the way to 0% at the horizon. As a consequence of this strong lensing, emitting objects that are contained within the photon orbit approximate the canonical pin-hole cavity example of a blackbody, becoming a perfect blackbody in the limit that the surface redshift goes to ∞ .

vide a mechanism to couple otherwise disparate regions of the photosphere. The travel times of these photons diverge only logarithmically with photosphere redshift, and therefore place an upper bound upon the equilibration timescale.

Inherent in these arguments is the assumption that *locally* the surface properties of any black hole alternative are not ill-behaved. That is, that the self-coupling is what determines the equilibration timescale. This may not be the case if, e.g., the heat capacity of the surface is effectively nearly infinite (or as in the case of a black hole, negative!). However, if the rate at which accreted baryonic material is incorporated into the surface is sufficiently slow, a baryonic atmosphere will develop. In this case, even for objects with near-vanishing temperature a hot atmosphere can be produced which satisfies the steady state condition.

2.3. Compact Objects & Blackbodies

Our argument will hinge upon our ability to specify the spectral signatures of any surface emission from black hole alternatives. Subject to the condition outlined in §2.2, it is natural to expect any such emission to be thermal. This is obvious if the object accrues an optically thick atmosphere of baryonic material. However, for any compact surface which lies within the photon orbit this is generally an excellent assumption.

By definition, at the photon orbit whether or not a pho-

ton impacts the surface is determined by the radial component of the momentum. Thus, if photons are emitted isotropically by a surface located at the photon orbit, half will impact the surface and half will escape to infinity. As the surface shrinks inside the photon orbit the fraction of escaping photons also decreases, falling to zero when the surface coincides with the horizon. Thus, the higher the redshift of the surface, the more effectively different regions on the surface are coupled to one another via radiation and the closer the surface approaches thermodynamic equilibrium. Consequently, high-redshift surfaces present a perverse realization of the canonical pin-hole cavity, becoming ideal blackbodies as z goes to ∞ (Broderick & Narayan 2006). For a Schwarzschild spacetime this is shown in Fig. 1; however this behavior is generic to spherically symmetric spacetimes. Thus if the system has sufficient time to have reached steady state, it must be a blackbody.

3. OBSERVATIONAL LIMITS UPON THE EXISTENCE OF HORIZONS

The primary astrophysical importance of a horizon is that the gravitational binding energy liberated by material as it accretes can be advected into the black hole without any further observational consequence. This is very different from accretion onto other compact objects, e.g., neutron stars, in which this liberated energy ultimately must be emitted by the stellar surface. Importantly, this argument is not dependent upon the particulars of the compact object. Any object powered by accretion, whose surface is visible from the external universe, should show evidence of surface radiation. We will use this fact to rule out the possibility that accreted material in Sgr A* settles in a region visible to outside observers, and in doing so make the argument that a horizon *must* exist. That is, we imagine that material comes to rest at some surface where it radiates its remaining kinetic energy and observationally constrain the associated surface luminosity.

The gravitational binding energy released by a particle falling onto the putative surface depends upon the details of the gravitational theory. For those theories which admit notions of energy conservation (in the test particle limit), including all stationary spacetimes, we may write this in terms of the specific binding energy at the putative surface, $\Delta\epsilon_g$. That is, the liberated energy due to a particle of mass m as measured at infinity is $E_\infty = \Delta\epsilon_g mc^2$. For a continuous accretion flow, this provides a total power, as measured at infinity, of

$$L_\infty = \Delta\epsilon_g \dot{M} c^2, \quad (1)$$

where \dot{M} is the mass accretion rate at the surface.

The particular form of $\Delta\epsilon_g$ also depends upon the nature of the accretion flow. For arbitrary stationary, spherically symmetric spacetimes this is computed in Appendix A for two typical cases: zero-angular momentum accretion flows in which matter does not orbit the black hole (e.g., Bondi accretion) and Keplerian accretion disk (e.g., appropriate for thin disks). In the latter case $\Delta\epsilon_g$ is generally smaller since a fraction of the liberated binding energy is necessarily converted into the kinetic energy associated with the orbital motion. Within the context of GR black holes⁴ $\Delta\epsilon_g$ is straightforward to compute

⁴ Throughout this section we will punctuate the analysis with

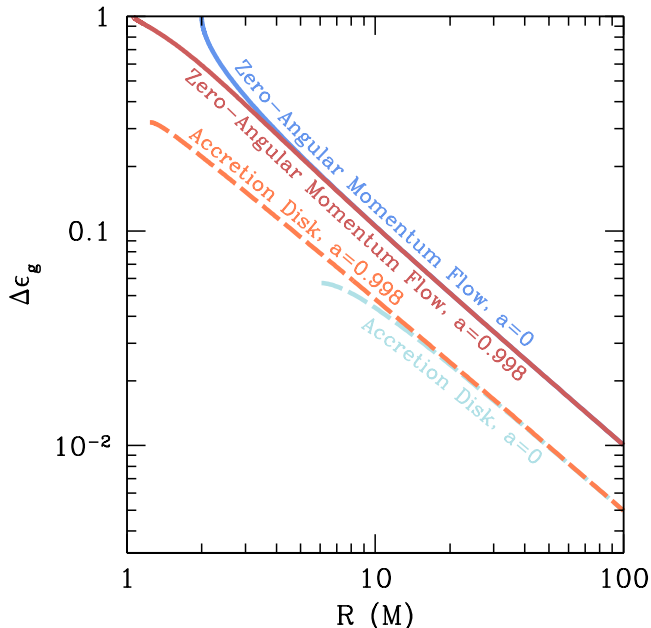


FIG. 2.— *Left*: Binding energy released per unit rest mass as a function of radius for material that has come to rest in the zero-angular momentum frame (*solid lines*) and the Keplerian frame (*dashed lines*) around a GR black hole. This is shown for a non-rotating GR black hole (Schwarzschild) by the blue lines and for a rapidly-rotating ($a = 0.998$) GR black hole (Kerr) by the orange lines. Note that in both cases, for the zero-angular momentum flow the entire rest mass is released at the horizon, while the energy released by an accretion disk peaks at the ISCO (inside of which no further stable orbits exist). Finally, beyond approximately $10M$, both follow their Newtonian expressions.

explicitly for these cases, and is shown in Fig. 2 for both nonrotating and rapidly-rotating black holes. However, we shall see that our ultimate constraints are independent of the form of $\Delta\epsilon_g$.

Only a fraction of L_∞ is converted into radiation. The observed electromagnetic luminosity at infinity may be parametrized in terms of a radiative efficiency, η_r :

$$L_{\text{obs}} = \eta_r L_\infty. \quad (2)$$

Gravitational binding energy may also be converted into the kinetic energy of relativistic outflows, which we similarly parametrize in terms of outflow efficiency, η_k :

$$L_{\text{out}} = \eta_k L_\infty. \quad (3)$$

It is important to note that η_r and η_k are primarily a function of the accretion flow, dependent upon the microphysics, and thus relatively insensitive to the character of strong gravity.

If a horizon is present, the remainder of L_∞ may be advected across it without further observational consequence. However, in the presence of a surface, if Sgr A* has reached steady state, this remainder must ultimately be radiated. Thus the surface luminosity, as measured at infinity, is

$$L_{\text{surf}} = L_\infty - L_{\text{obs}} - L_{\text{out}} = \frac{1 - \eta_r - \eta_k}{\eta_r} L_{\text{obs}}, \quad (4)$$

examples from GR black holes. However, it should be understood that our analysis is independent of these specific examples, and in fact considerably more general.

Where we have written this entirely in terms of the unknown efficiencies and the observed luminosity. (Specifically, note that neither $\Delta\epsilon_g$ nor \dot{M} appear in this expression.)

As we have argued in §2.3, for compact surfaces this radiation will be in the form of a blackbody spectrum. That is, in terms of the apparent radius (R_a) and temperature (T_∞) of the putative surface, as measured at infinity,

$$L_{\text{surf}} = 4\pi\sigma R_a^2 T_\infty^4. \quad (5)$$

Alternatively, this provides a means to estimate the surface temperature (and thus spectrum) given L_{surf} and R_a . Combined with eq. (4), we may write T_∞ in terms of L_{obs} , R_a , η_r and η_k :

$$T_\infty = \left(\frac{1 - \eta_r - \eta_k}{\eta_k} \frac{L_{\text{obs}}}{4\pi\sigma R_a^2} \right)^{1/4}. \quad (6)$$

In terms of this surface temperature, the expected flux seen by distant observers is then

$$F_\nu = \pi \left(\frac{R_a}{D} \right)^2 B_\nu(T_\infty), \quad (7)$$

where B_ν is the blackbody spectrum.

However, no thermal surface component is observed in Sgr A*'s spectrum. Thus, if such surface emission is present, it must be hidden under the emission from the accretion flow. As a consequence, each flux measurement constitutes an independent upper limit upon the surface flux, and thus surface temperature. Explicitly, given an observed flux F_ν^{obs} , $T_\infty \leq T_{\text{max}}(\nu, F_\nu^{\text{obs}}, R_a/D)$ where

$$T_{\text{max}} \left(\nu, F_\nu^{\text{obs}}, \frac{R_a}{D} \right) = h\nu / k \ln \left(1 + \frac{2\pi h\nu^3 R_a^2}{c^2 F_\nu^{\text{obs}} D^2} \right). \quad (8)$$

Note that this is generally a function of R_a , a consequence of the fact that larger surfaces are correspondingly cooler, and therefore easier to hide under the observed emission.

This maximum temperature then implies a limit upon L_{surf} directly via the black body condition:

$$\frac{L_{\text{surf}}}{L_{\text{obs}}} \leq \frac{L_{\text{surf,max}}}{L_{\text{obs}}} \equiv \frac{\sigma R_a^2}{D^2 F_{\text{obs}}} T_{\text{max}}^4 \left(\nu, F_\nu^{\text{obs}}, \frac{R_a}{D} \right), \quad (9)$$

where $F_{\text{obs}} = L_{\text{obs}}/4\pi D^2$ is the integrated observed flux from Sgr A*. Alternatively, we may rewrite this in terms of a *lower* limit upon the efficiencies:

$$\eta_r + \eta_k \geq \frac{1}{1 + L_{\text{surf,max}}/L_{\text{acc}}}. \quad (10)$$

That is, if the efficiencies are sufficiently high the unradiated liberated energy in the accretion flow is sufficiently small that the surface could escape detection. Unlike $L_{\text{surf}}/L_{\text{acc}}$, we have natural scales against which to compare $\eta_r + \eta_k$. In prodigiously accreting systems, such as active galactic nuclei, X-ray binaries & gamma-ray bursts, which are believed to be radiatively efficient, the radiative efficiency $\eta_r + \eta_k$ is estimated to be $\sim 10\%$ (Kato et al. 2008). In Sgr A*, on the other hand, η_r is thought to be quite small (0.01–1% for typical accretion models) as a consequence of the weak coupling between accreting ions and electrons within the gas (Narayan & McClintock 2008), and there is presently no direct evidence for energetic outflows.

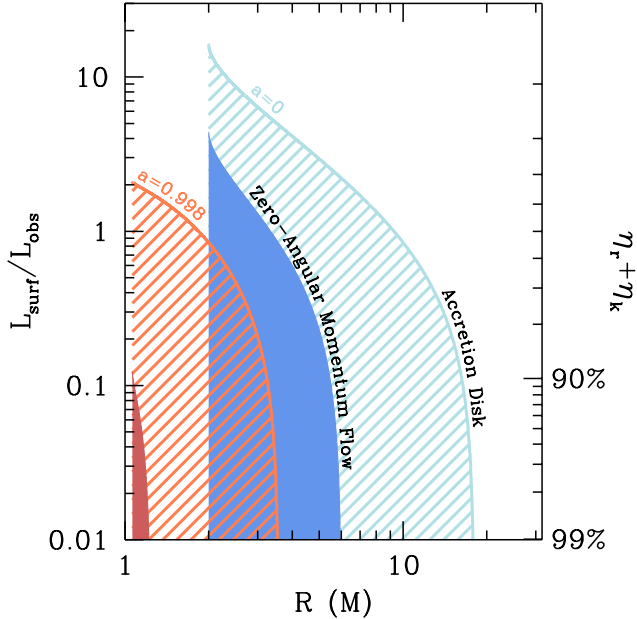


FIG. 3.— Fundamental constraints upon $L_{\text{surf}}/L_{\text{obs}}$ (or $\eta_r + \eta_k$) in GR black hole spacetimes as a function of the coordinate radius of the stopping region. In the shaded/hatched regions $\eta_r + \eta_k > \Delta\epsilon_g(R)/\Delta\epsilon_g(r_{\text{ISCO}})$ and are thus not possible in the context of GR accretion theory. This is shown for when the accreted material comes to rest in the zero-angular momentum frame and the Keplerian frame around non-rotating and rapidly-rotating ($a = 0.998$) black holes. In all cases, the shaded regions are truncated at the coordinate position of the relevant horizons and the excluded $L_{\text{surf}}/L_{\text{obs}}$ vanishes at some radii, which is a natural result of fixing r_{ISCO} (for the zero-angular momentum flow, this happens at r_{ISCO} itself).

Within the context of GR black holes and standard accretion theory, there are fundamental limits upon how large $\eta_r + \eta_k$ may be for compact surfaces. This arises from the fact that matter inside of the Innermost Stable Circular Orbit (ISCO) plunges rapidly onto the surface, and thus does not have sufficient time to radiate. In contrast, outside of the ISCO material may linger on stable orbits for long periods of time, and at least in principle can radiate efficiently. Thus, even if the “intrinsic” radiative efficiency outside of the ISCO reached unity, the accreting material would still accrue additional kinetic energy during the plunge from the ISCO to the putative surface. If this surface is located inside of the ISCO, we may therefore place a lower bound upon the additionally liberated energy, and thus an upper bound upon $\eta_r + \eta_k$. These are shown in Fig. 3 for zero-angular momentum accretion flows⁵ and orbiting accretion disks surrounding both non-rotating and rapidly-rotating black holes (see Appendix A for details). For orbiting disks the maximum value of $\eta_r + \eta_k$ is generally less than 33%.

Therefore, each combined size and flux measurement of Sgr A* places a direct constraint upon the luminosity of a putative surface, or, equivalently, upon the radiative efficiency of the accretion flow. Thus, we now turn our attention to describing the current best constraints upon

⁵ Note that we are being maximally conservative by assuming that a zero-angular momentum flow can radiate all its binding energy down to the ISCO. Models of non-rotating accretion flows are usually very radiatively inefficient. Allowing for this would strengthen our argument substantially.

TABLE 1
VLBI SIZE CONSTRAINTS

λ (mm)	R_a (μas) ^a	$3\text{-}\sigma R_a$ (μas) ^b	Ref.
1.3	19	27	Doeleman et al. (2008)
3	63	84	Shen et al. (2005)
7	120	150	Bower et al. (2004)

^a The measured half-width, half-max

^b The $3\text{-}\sigma$ upper limit upon the half-width, half-max

TABLE 2
DEREDDENED INFRARED FLUX LIMITS

Band	λ (μm)	F_ν (mJy) ^a	Ref.
<i>H</i>	1.6	2.60 ± 0.28	Hornstein et al. (2007)
<i>K'</i>	2.1	1.66 ± 0.18	Hornstein et al. (2007)
<i>L'</i>	3.8	1.28 ± 0.30	Ghez et al. (2005)
<i>M_S</i>	4.7	2.2 ± 1.6	Hornstein et al. (2007)
<i>N</i>	8.7	22 ± 14	Schödel et al. (2007)

^a The uncertainty in F_ν is taken to be the $1\text{-}\sigma$ detection uncertainty.

R_a/D and F_ν^{obs} .

3.1. Millimeter Size Constraints

Measuring the intrinsic size of Sgr A* is complicated by its low luminosity, exceedingly small size, interstellar scattering and the opacity of the surrounding accretion flow. As a result, high-frequency VLBI has produced the only meaningful limits upon the size of a putative surface. Recent measurements of the photosphere radius (half-width, half-max) are listed in Table 1.

At wavelengths longer than 1.3 mm Sgr A* is optically thick and the observed size is dominated by interstellar scattering, requiring a careful subtraction of the empirically determined scattering law. However, at 1.3 mm interstellar scattering is subdominant and the plasma surrounding Sgr A* has become optically thin. Perhaps surprisingly, at this wavelength the inferred angular size, $37 \pm 11 \mu\text{as}$, is *smaller* than the apparent diameter of the horizon ($48\text{--}55 \mu\text{as}$ depending upon spin), *independent of black hole spin* (Doeleman et al. 2008). However, this is natural in the context of an orbiting accretion flow or an outflow; in both cases the image is dominated by the approaching plasma (Broderick et al. 2008; Broderick & Loeb 2008). Therefore, the measured $37 \pm 11 \mu\text{as}$ may not represent R_a/D of the surface itself, but instead result from the velocity structure of the accreting material. Nevertheless, efforts to fit this result using existing accretion models for Sgr A* imply that the surface lies within the photon orbit.

3.2. Infrared Flux Limits

Given the size limits, typical values of T_∞ range from $10^2\text{--}10^4$ K, and thus the emission from a putative surface peaks in the near and mid-infrared. Fortunately, despite the large infrared extinction in the direction of the Galactic center, there are a number of observations of Sgr A* at these wavelengths. Furthermore, there exists an accurate empirically determined extinction law for this region (Moneti et al. 2001), making it possible to deredden the observed fluxes, producing intrinsic infrared flux measurements for Sgr A*.

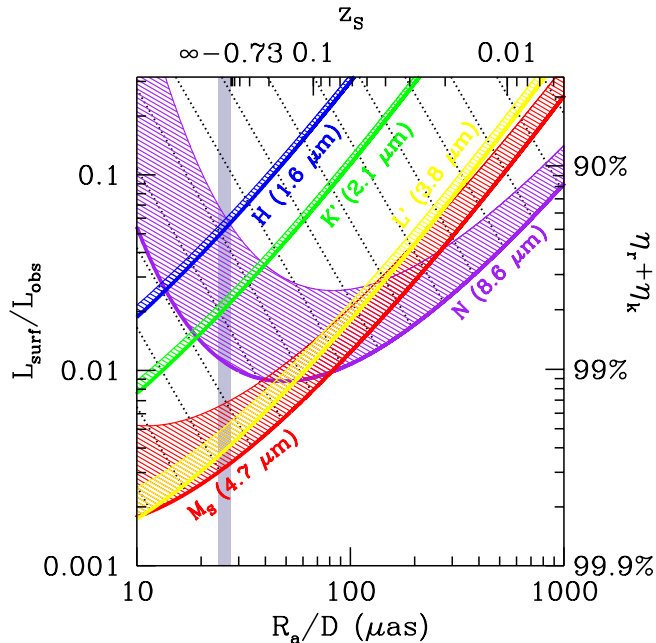


FIG. 4.— The limits upon $L_{\text{surf}}/L_{\text{obs}}$ implied by eq. (9) as a function of the photosphere size as seen at infinity for the infrared measurements listed in Table 2. The hatched bands denote the $3\text{-}\sigma$ upper-bounds. The peculiar behavior of the N -band constraint is a result of the transition from the Rayleigh-Jeans limit to the Wien limit around $R_a/D \simeq 50 \mu\text{as}$ as the surface becomes cooler. The region above any of the limits is necessarily excluded. The right-hand vertical axis shows the corresponding limits upon the accretion flow’s radiative efficiencies. The top axis gives the redshift associated with a Schwarzschild spacetime given the apparent source radius and the thick grey line shows the apparent radii associated with the photon orbit for Kerr spacetimes.

However, in these bands the emission from Sgr A* is dominated by variability (see, e.g., Hornstein et al. 2007), which must clearly be associated with the accretion flow and not the surface. This prevents an unambiguous detection of quiescent emission. Therefore, the flux limits we collect in Table 2 are determined by inspecting variable infrared light curves and extracting the lowest flux detection. The L' ($3.8 \mu\text{m}$) and N ($8.7 \mu\text{m}$) band limits are taken directly from Ghez et al. (2005) and Schödel et al. (2007), respectively. The H ($1.6 \mu\text{m}$), K' ($2.1 \mu\text{m}$) and M_S ($4.8 \mu\text{m}$) band limits were determined by examining the panels of Fig. 2 of Hornstein et al. (2007), which show dereddened flux light curves for a number of infrared flares in Sgr A* and a variety of near-infrared bands.

3.3. Constraints Upon Surface Existence

Each of the infrared flux limits listed in Table 2 places an upper limit upon $L_{\text{surf}}/L_{\text{obs}}$ via eq. (9), given a value of R_a . Fig. 4 shows these limits as a function of surface size, together with their $3\text{-}\sigma$ upper bounds (denoted by the hatched regions). Generally, larger surfaces are cooler. This has two consequences. First, since the strongest constraints are placed by flux measurements near the peak in the thermal spectrum, the infrared band providing the most stringent limit is a function of R_a as well; near $R_a/D \simeq 100 \mu\text{as}$ the infrared band dominating

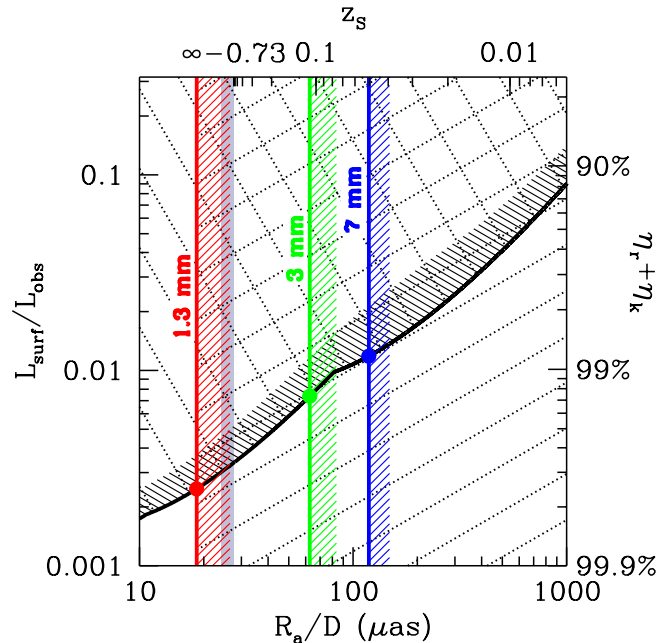


FIG. 5.— The limits upon R_a/D implied by recent VLBI observations listed in Table 1, overlaid upon the combined constraint implied by IR flux measurements. Regions to the right of the left-most (smallest) size constraint are excluded. When combined with the limits from the IR flux measurements, the permissible parameter space is reduced to a small corner in the R_a - $L_{\text{surf}}/L_{\text{obs}}$ plane. The axes are identical to those in Fig. 4.

the constraint changes from M_S ($4.7 \mu\text{m}$)⁶ to N ($3.8 \mu\text{m}$). The constraint due to the combination of all of the infrared bands is the lower-envelope of all the bands, and defines the excluded region, corresponding to small, luminous surfaces. Second, since cooler surfaces are more easily masked by the emission from the accretion flow, the limit becomes less stringent as R_a increases. Thus, the infrared constraint upon $L_{\text{surf}}/L_{\text{obs}}$ must be supplemented with an independent limit upon the size of the putative surface.

Upper limits upon R_a/D are found directly via the radio VLBI observations collected in Table 1. These are shown in Fig. 5, with their $3\text{-}\sigma$ upper bounds (again denoted by the hatched regions) together with the combined infrared limit. The recent 1.3 mm detection is the strongest, and excludes $R_a/D > 27 \mu\text{as}$ at the $3\text{-}\sigma$ level. When combined with the infrared constraints, only a small corner of the R_a - $L_{\text{surf}}/L_{\text{obs}}$ is still permitted, corresponding to small, dim surfaces. Earlier measurements at 7 mm and 3 mm already required $L_{\text{surf}}/L_{\text{obs}} \lesssim 0.02$. The new 1.3 mm detection improves these by nearly an order of magnitude, requiring $L_{\text{surf}}/L_{\text{obs}} \lesssim 0.004$ at the $3\text{-}\sigma$ level.

A more physical interpretation is provided by the accretion efficiencies the latest observations now demand, shown on the right-hand vertical axis. In order for a surface to be present $\eta_r + \eta_k \gtrsim 99.6\%$ (at $3\text{-}\sigma$)! That is, as matter falls onto Sgr A*, somehow 99.6% of the liberated gravitational binding energy must be radiated, powering

⁶ Though the small uncertainties associated with the L' ($3.8 \mu\text{m}$) measurement dominate the uncertainties at low R_a despite the fact that the limit derived from the best estimate of the M_S -band flux is always stronger.

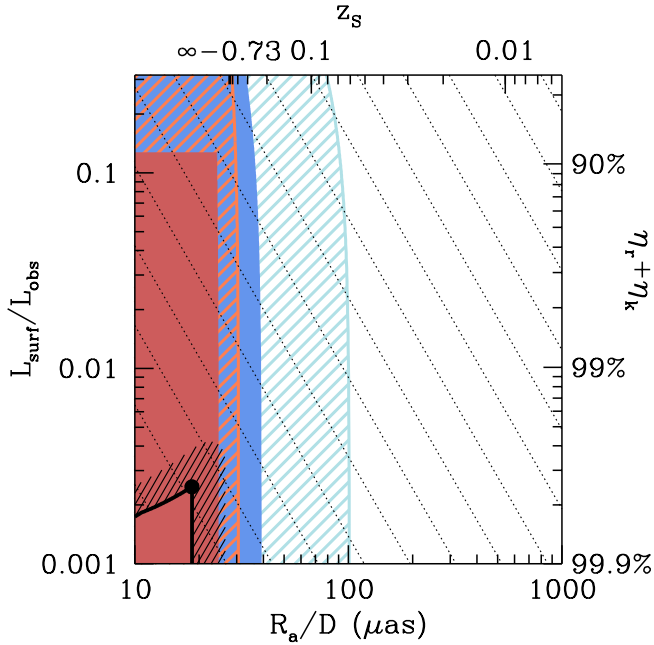


FIG. 6.— The combined limits upon $L_{\text{surf}}/L_{\text{obs}}$ and R_a/D compared with the regions generally excluded in GR black hole spacetimes (shown as a function of coordinate radius in Fig. 3). Extending these to angular scales smaller than the theoretical minimum (the angular size of the horizon) results in the rectangular appearance. Blue and red excluded regions correspond to Schwarzschild and maximal-Kerr black holes, respectively. Hatched and solid limits correspond to Keplerian and zero-angular momentum accretion flows, respectively. Given the most recent infrared flux limits and mm-VLBI size constraints, $\eta_r + \eta_k$ is inconsistent by more than an order of magnitude with estimates for Sgr A* specifically, relativistic accretion flows generally and even fundamental limits in GR spacetimes. The axes are identical to those in Fig. 4.

either the observed luminosity or kinetic outflows. Otherwise the emission of the remainder upon settling onto the surface would have been detected. This needed efficiency is considerably larger than even the 10% efficiencies implicated in rapidly accreting systems, let alone the meager efficiencies (0.01 – 1%) inferred in Sgr A*.

More striking is the comparison of this to the *maximum* efficiencies within GR spacetimes. A variety of black hole alternatives are grafted onto such spacetimes outside of some compact region, and thus in these the GR limits explicitly hold. For other black hole alternatives, including those associated with different gravity theories, these limits at least provide a scale for comparison. These fundamental constraints upon the efficiencies arise from the fact that accreting material cannot radiate efficiently inside of the innermost stable circular orbit (ISCO). Inside of the ISCO accreting material plunges inward rapidly in comparison to the radiative timescales. Thus, *even if the intrinsic radiative efficiency outside the ISCO is 100%* (which is extremely unlikely), the fraction of the total binding energy released by accreting gas in the course of its inward flow is limited to that fraction that is emitted outside the ISCO. Therefore, within the context of GR, even with the most conservative of assumptions (zero-angular momentum accretion flow with 100% radiative

efficiency down to the ISCO) we obtain an absolute upper limit on $\eta_r + \eta_k$ for surfaces which lie within the photon orbit of 91%, while for a more reasonable accretion scenario involving orbiting gas the limit is 33% (see Appendix A for more details). The combined observational limits upon $L_{\text{surf}}/L_{\text{acc}}$ and $\eta_r + \eta_k$ are compared against those inferred in GR spacetimes for zero-angular momentum and Keplerian flows in Fig. 6. In particular, there is no longer any allowed region given the recent 1.3 mm size constraint.

4. CONCLUSIONS

Recent infrared and mm-VLBI observations imply that if the matter accreting onto Sgr A* comes to rest in a region visible to distant observers, the luminosity associated with the surface emission from this region satisfies $L_{\text{surf}}/L_{\text{acc}} \lesssim 0.003$. Equivalently, these observations require that 99.6% of the gravitational binding energy liberated during infall is radiated in some form prior to finally settling. These numbers are inconsistent by orders of magnitude with our present understanding of the radiative properties of Sgr A*'s accretion flow specifically and relativistic accretion flows generally. Therefore, it is all but certain that no such surface can be present, i.e., *an event horizon must exist*.

Critical to our analysis is the recent sub-mm constraint upon the size of the emitting region of Sgr A* since it: (1) justifies the assertion that the putative photosphere is sufficiently compact to be treated as a blackbody, (2) limits the photosphere's temperature from below, and (3) within the context of GR provides a strong constraint upon possible values of the radiative efficiency that is easily excluded. Future mm-VLBI observations will be critical to understanding the morphology of Sgr A*'s emitting region, and thus validating the interpretation of current observations as the approaching side of an orbiting accretion flow, with the attendant implications for Sgr A*'s size. However, unless the spacetime around Sgr A* deviates substantially from that of a GR black hole, future observations of the intrinsic size of Sgr A* will be unable to further restrict the size of a putative surface due to the influence of gravitational lensing. The reason is that all objects which lie within the photon orbit generally have the same apparent radius. Thus, obtaining more sensitive near-infrared flux measurements will remain a crucial avenue for strengthening this kind of argument.

We were able to place these constraints completely in terms of observable quantities: fluxes and the apparent size of Sgr A*. Beyond using GR spacetimes to provide scales for the purpose of comparison, we did not need to make use of the particular structure of GR black hole spacetimes. As a result, our conclusions may be applied more generally to all gravitational theories that admit notions of energy conservation in the test-particle limit. Specifically, these include all geometric gravitational theories that admit stationary solutions, including all of the $f(R)$ theories and black hole alternatives that exist within the context of GR. As a consequence, we cannot yet say that Sgr A* is described by a GR black hole despite being able to conclude that a horizon must exist.

APPENDIX

GRAVITATIONAL BINDING ENERGY IN STATIONARY SPACETIMES

As material falls into the the gravitational potential well induced by Sgr A* it necessarily converts a portion of its gravitational binding energy into luminosity. In §3 we simply parametrized the amount of liberated energy in terms of some $\Delta\epsilon_g$, finding it unnecessary to specify this function further. In this appendix we derive a general expression for the magnitude of the binding energy available. We necessarily assume that gravity is described by a metric theory, and that this theory admits a stationary solution. For simplicity, we will not explicitly discuss non-spherical solutions, however this makes no formal difference. We take the metric signature to be $-+++$ and choose units such that $G = c = 1$.

The state of an infalling particle, characterized by its 4-momentum, p^μ , can be used to determine the energy available to radiation as measured at infinity. Given an initial momentum for an infalling particle, p_i^μ , the momentum of the radiated photon, p_γ^μ , and the final particle momentum, p_f^μ , conservation of momentum gives

$$p_\gamma^\mu = p_i^\mu - p_f^\mu. \quad (\text{A1})$$

The steady state of the spacetime implies that along geodesics (e.g., the null geodesic followed by the photon, or the free-fall of the gas particle) p_t is explicitly conserved, corresponding to a conserved energy. Thus, the photon's energy at infinity is simply $\Delta\epsilon_g \equiv -p_{\gamma t} = p_{f t} - p_{i t}$. Since this quantity is observed at infinity, where the spacetime is flat, we are guaranteed that this quantity is not affected by the choice of coordinates deep in the gravitational well. In addition, this has the virtue of being precisely what is measured.

We will consider two scenarios, corresponding to different choices of p_f^μ . The first of these is the most extreme: the particle was initially at rest at infinity ($p_{i t} = -m$), fell to some radius and came to rest, with ⁷

$$p_\mu^{\text{rest}} = \left(\frac{m}{\sqrt{-g^{tt}}}, 0, 0, 0 \right), \quad (\text{A2})$$

at which point its accumulated binding energy was emitted. The available energy, per unit mass is then

$$\Delta\epsilon_g = \frac{p_t - p_t^{\text{rest}}}{m} = \frac{\sqrt{-g^{tt}} - 1}{\sqrt{-g^{tt}}} = \frac{z}{z + 1}, \quad (\text{A3})$$

where the redshift is defined in the usual way: $z \equiv \sqrt{-g^{tt}} - 1$.

Our second scenario involves the presence of an accretion disk. Previously, we assumed that the accreting material has no angular momentum, and therefore explicitly ignored orbital motion. Generally, the gas is expected to orbit the black hole, and the kinetic energy in the orbital motion will be supplied by the liberated gravitational binding energy, decreasing the reservoir of energy available to radiation. Hence we have placed a firm upper limit upon the luminosity of the accretion flow itself. However, we can compute the decrease explicitly for the simple case of stationary, spherically symmetric spacetimes. If

$$ds^2 = g_{tt}dt^2 + g_{rr}dr^2 + r^2d\Omega^2, \quad (\text{A4})$$

for orbits in the equatorial plane, p_t^{orbit} and p_ϕ^{orbit} are conserved, p_{orbit}^θ vanishes due to symmetry and,

$$p_{\text{orbit}}^r = m \frac{dr}{d\tau} = \sqrt{-\frac{1}{g_{rr}} \left(m^2 + g^{tt} p_t^{\text{orbit}2} + \frac{p_\phi^{\text{orbit}2}}{r^2} \right)} = 0. \quad (\text{A5})$$

If the orbit is to remain closed, we also require

$$m \frac{d^2r}{d\tau^2} = -\frac{1}{2} \frac{\partial}{\partial r} \frac{1}{g_{rr}} \left(m^2 + g^{tt} p_t^{\text{orbit}2} + \frac{p_\phi^{\text{orbit}2}}{r^2} \right) = 0. \quad (\text{A6})$$

Solving these for p_t^{orbit} and p_ϕ^{orbit} gives

$$p_t^{\text{orbit}} = \frac{1}{\sqrt{-g^{tt}}} \Big/ \sqrt{1 - \frac{1}{2} \frac{\partial \ln(-g^{tt})}{\partial \ln r}} = \frac{1}{z + 1} \Big/ \sqrt{1 + \frac{\partial \ln(z + 1)}{\partial \ln r}}, \quad (\text{A7})$$

which is generally larger than for the zero-angular momentum case (since z generally decreases with radius). Correspondingly, $\Delta\epsilon_g$ in this case is generally lower.

While our discussion of the liberated gravitational binding energy is quite general, requiring only that gravity is described by a metric theory that admits a stationary solution, GR can provide some intuition regarding the magnitude of energy that can reasonably be released. Fig. 2 shows the specific binding energy released by material as a function

⁷ This corresponds to the momentum of an observer that has freely fallen from infinity and decelerated only along the direction of motion. In the context of general relativity this choice of rest frame corresponds to the Zero Angular Momentum Observer for rotating black holes; however, this expression is completely general.

of radius. Typically, the ISCO is the final radius at which matter can efficiently radiate since inside this point material plunges into the black hole on a free fall timescale⁸, rapid in comparison to the relevant radiative timescale for the rather pedestrian densities and magnetic fields observed in Sgr A*⁹. As a consequence, *even if 100% of the gravitational binding energy released outside of the ISCO is radiated or goes into outflows*, the maximum fraction of the rest mass that can be emitted is shown by the blue line in Fig. 2. If the region where the accreted material finally comes to rest lies within the ISCO, additional gravitational binding energy will be released, and must subsequently be radiated in the stopping region. Thus, the radiative efficiency of the accretion flow, defined by

$$\eta_r + \eta_k \equiv \frac{L_{\text{acc}}}{\Delta\epsilon_g(R)\dot{M}} + \frac{L_{\text{out}}}{\Delta\epsilon_g(R)\dot{M}} \quad (\text{A8})$$

must satisfy

$$\eta_r + \eta_k \leq \frac{\Delta\epsilon_g(r_{\text{ISCO}})}{\Delta\epsilon_g(R)} \quad (\text{A9})$$

where R is the radius of the stopping region. This limit shown as a function of R in Fig. 3 for zero-angular momentum accretion flows and accretion disks in Schwarzschild and Kerr spacetimes. Generally, once R is constrained to lie within the photon orbit, the maximum $\eta_r + \eta_k$ possible is 91%, corresponding to a zero-angular momentum accretion flow in a rapidly-rotating ($a = 0.998$) Kerr spacetime. When an accretion disk is present this limit declines to 33%. For the Schwarzschild spacetime, $\eta_r + \eta_k$ is bounded from above by 43% (zero-angular momentum accretion) and 14% (accretion disk). In all cases, these maximum values are substantially smaller than the limits set by recent sub-mm and infrared observations if Sgr A* did not have a horizon.

APPARENT SIZES OF COMPACT OBJECTS

Observations of the size of a compact emitting region is necessarily impacted by strong gravitational lensing. In metric theories of gravity, objects associated with deep potential wells will appear larger to observers at infinity. The apparent size of the region is directly related to both the physical size and the redshift of the compact object. Thus, relating the actual size of a compact emitting region to the observed size requires some understanding of the spacetime structure around the object. This is, of course, one of the reasons we chose to cast the constraints upon the existence of a horizon, described in §3, in terms of R_a and not a physical object size. Nevertheless, for completeness, we discuss the procedure here.

It is typically very difficult to compute the relationship between the physical and observed size and shape of a compact emitting object. However, in the special case of a spherically symmetric spacetime, this is generally tractable, independent of the particular form of the metric. We assume

$$ds^2 = g_{tt}dt^2 + g_{rr}dr^2 + r^2d\Omega^2, \quad (\text{B1})$$

where g_{tt} and g_{rr} are functions of r alone. Then, in the equatorial plane, the null geodesics are defined by

$$\frac{dt}{d\lambda} = g^{tt}, \quad \frac{dr}{d\lambda} = \sqrt{\frac{1}{g_{rr}} \left(-g^{tt} - \frac{b^2}{r^2} \right)} = \sqrt{\frac{-g^{tt}}{g_{rr}} \left[1 - \frac{b^2}{(z+1)^2 r^2} \right]}, \quad \frac{d\theta}{d\lambda} = 0 \quad \text{and} \quad \frac{d\phi}{d\lambda} = \frac{b}{r^2}, \quad (\text{B2})$$

where the equations for $dt/d\lambda$ and $d\phi/d\lambda$ are associated with the existence of a time-like and azimuthal Killing vectors, respectively, the equation for $d\theta/d\lambda$ is fixed by vertical symmetry and the equation for $dr/d\lambda$ arises from the null ray condition. In these b is the impact parameter at infinity and λ is an arbitrary affine parameter. The minimum radius reached by a given null geodesic occurs at its inner turning point, at which $b = r\sqrt{-g^{tt}} = r(z+1)$. Alternatively, this corresponds to the maximum b that a null geodesic can have and still impact a surface of radius r . Thus, the apparent radius, R_a , of an object with physical radius R is simply

$$R_a = R(z+1). \quad (\text{B3})$$

Some care must be taken, however, when R is smaller than the photon orbit. This is because rays which cross the photon orbit have no radial turning points, and therefore will in all cases be captured. This is clear from the definition of the photon orbit, r_γ :

$$\left. \frac{d}{dr} \frac{1}{(z+1)^2 r^2} \right|_{r_\gamma} = 0, \quad (\text{B4})$$

⁸ In the context of thin disks this corresponds to the zero-torque inner-boundary condition, which has been well tested by the fitting of X-ray spectra from X-ray binaries. In the context of thick disks, or quasi-spherical accretion flows, in principle magnetic fields can couple material inside of the ISCO to the flow outside, transferring energy in the process. However, thick disks are thick *because* $\eta_r \lesssim 0.1$, limiting the ability of the disk to cool efficiently. Thus, even in the presence of substantial magnetic coupling, thick disks are also bounded by this limit.

⁹ In order to reach $\eta_r + \eta_k \simeq 1$ the energy of the accreting material must be extracted over the timescale comparable to the free-fall timescale at the point where $\eta_r + \eta_k$ of the binding energy has been released. That is, because the liberated binding energy rapidly increases as material falls inward, $\eta_r + \eta_k$ is determined by the last radius at which energy extraction can keep pace with the infall. Explicitly, for a Schwarzschild black hole this implies that the cooling timescale must be less than $(1 - \eta_r - \eta_k)\Delta\epsilon_g / (d\Delta\epsilon_g/d\tau) = 2R(R/2M)^{3/2} \sqrt{1 - 2M/R} (1 - \eta_r - \eta_k)$. For $\eta_r + \eta_k = 99.6\%$, this corresponds to cooling timescales of 2 s at $R = 6M$ and 0.3 s at $R = 3M$, both of which are only realized in practice in extraordinarily dense environments such as newly formed neutron stars.

which corresponds to the position of the maximum of the “effective potential” in the radial equation. Thus, if

$$b < r_\gamma \left[z(r_\gamma) + 1 \right] \quad \Rightarrow \quad \frac{b^2}{(z+1)^2 r^2} < 1 \quad \text{for all } r. \quad (\text{B5})$$

As a consequence, the apparent radius of objects for which $R < r_\gamma$ is the same as that for objects with $R = r_\gamma$. Thus, generally,

$$R_a = \begin{cases} r_\gamma \left[z(r_\gamma) + 1 \right] & \text{if } R \leq r_\gamma \\ R \left[z(R) + 1 \right] & \text{otherwise.} \end{cases} \quad (\text{B6})$$

In the case of the Schwarzschild metric, this gives the well-known result

$$R_a = \begin{cases} 3\sqrt{3}M & \text{if } R \leq 3M \\ R\sqrt{\frac{R}{R-2M}} & \text{otherwise.} \end{cases} \quad (\text{B7})$$

For a rapidly rotating Kerr spacetime, the apparent radius in the equatorial plane may also be computed without undue difficulty (though in this case care must be taken into account for the non-diagonal components of the metric). Generally, this is given by

$$R_a = \frac{1}{2} (b_+ - b_-), \quad (\text{B8})$$

where

$$b_\pm = \pm \max \left(R \frac{R\sqrt{R^2 - 2MR + a^2} \mp 2aM}{R^2 - 2MR}, r_{\pm\gamma} \frac{r_{\pm\gamma} \sqrt{r_{\pm\gamma}^2 - 2Mr_{\pm\gamma} + a^2} \mp 2aM}{r_{\pm\gamma}^2 - 2Mr_{\pm\gamma}} \right) \quad (\text{B9})$$

in which $r_{\pm\gamma}$ is the radius of the prograde/retrograde photon orbit. Since these differ for rotating black holes, we generally have three conditions. In the case of a maximally rotating black hole ($a = 1$), this expression is especially simple:

$$R_a = \begin{cases} \frac{9}{2}M & \text{if } R \leq r_{+\gamma} \\ \frac{R + 8M}{2} & \text{if } r_{+\gamma} < R \leq 4M \\ R\frac{R-1}{R-2} & \text{otherwise,} \end{cases} \quad (\text{B10})$$

where R is the object radius in Boyer-Lindquist coordinates. While $r_{+\gamma} = M$ in these coordinates for $a = 1$, there remains a finite proper distance between the photon orbit and the horizon, the equality being an artifact of the coordinates themselves. For this reason, we distinguish between these formally, though it makes no difference (since $R_a = 9/2$ for all R between $r_{+\gamma}$ and the horizon), as it must not given that R_a is a gauge invariant quantity as a consequence of its definition.

Most important for the present discussion is the fact that R_a for the Schwarzschild and equatorial Kerr spacetimes differs by only about 15%. Thus, despite the vastly different coordinate sizes, an object with $R = 1M$ embedded in a maximal Kerr spacetime has roughly the same apparent size as an object with $R = 3M$ embedded in a Schwarzschild spacetime. As a consequence, if the present limit upon the size of the sub-mm emitting region in Sgr A* of $37 \mu\text{as}$ ($R_a = 3.5M$) is interpreted as a photosphere surrounding the stopping region, it constrains the size of a central emitting region to lie well within the photon orbit of both a Kerr and Schwarzschild black hole.

On the other hand, the anomalously small apparent radius might appear unphysical within the context of GR. However, this is easily rectified if the emission region is interpreted instead as the visible arc of an oncoming accretion disk (as a result of Doppler boosting and Doppler shifts, the receding side being considerably dimmer for the same reason, Broderick & Loeb 2006a). While the equatorial extent of the arc can be significantly smaller than the minimum apparent radius in this situation, the vertical extent is still roughly $2R_a$ (Broderick et al. 2008; Broderick & Narayan 2006, see, e.g.,). Hence, unless the projected baseline was extraordinarily fortuitously aligned, again we would expect large measured sizes for central emission regions larger than the photon orbit radius. It is possible to coincidentally fit the existing spectral, polarization and mm-VLBI observations using orbiting accretion flow models (Broderick et al. 2008). However, this is due at least in part to the fact that the existing mm-VLBI size constraint is essentially restricted to the East-West direction. Future mm-VLBI observations will be critical to unambiguously determining the morphology of the emitting region (Fish et al. 2009).

REFERENCES

- Agol, E. 2000, *ApJ*, 538, L121
- Aitken, D. K., Greaves, J., Chrysostomou, A., et al. 2000, *ApJ*, 534, L173
- Blandford, R. D. & Begelman, M. C. 1999, *MNRAS*, 303, L1
- Bower, G. C., Wright, M. C. H., Falcke, H., & Backer, D. C. 2003, *ApJ*, 588, 331
- Bower, G. C. et al. 2004, *Science*, 304, 704
- Bower, G. C. et al. 2006, *ApJ*, 648, L127
- Broderick, A. & Loeb, A. 2008, *ApJ* (*submitted, arXiv:0812.0366*)
- Broderick, A. E., Fish, V. L., Doeleman, S. S., & Loeb, A. 2008, *ApJ* (*submitted, arXiv:0809.4490*)
- Broderick, A. E. & Loeb, A. 2005, *MNRAS*, 363, 353
- Broderick, A. E. & Loeb, A. 2006a, *ApJ*, 636, L109
- Broderick, A. E. & Loeb, A. 2006b, *MNRAS*, 367, 905
- Broderick, A. E. & Narayan, R. 2006, *ApJ*, 638, L21
- Broderick, A. E. & Narayan, R. 2007, *Class. Quantum Grav.*, 24, 659
- Doeleman, S. S. et al. 2008, *Nature*, 455, 78
- Falcke, H., Melia, F., & Agol, E. 2000, *ApJ*, 528, L13
- Fish, V. L., Broderick, A. E., Doeleman, S. S., & Loeb, A. 2009, *ApJ*, 692, L14
- Ghez, A. M. et al. 2005, *ApJ*, 635, 1087
- Ghez, A. M. et al. 2008, arXiv:0808.2870v1 [astro-ph]
- Gillessen, S. et al. 2008, arXiv:0810.4674 [astro-ph]
- Hawking, S. W. 2005, *Phys. Rev. D*, 72, 084013
- Heger, A. et al. 2003, *ApJ*, 591, 288
- Hornstein, S. D. et al. 2007, *ApJ*, 667, 900
- Kato, S., Fukue, J., & Mineshige, S. 2008, *Black-Hole Accretion Disks* (Kyoto University Press)
- Krichbaum, T. P. et al. 2006, *Journal of Physics Conference Series*, 54, 328
- Macquart, J.-P. et al. 2006, *ApJ*, 646, L111
- Marrone, D. P., Moran, J. M., Zhao, J.-H., & Rao, R. 2006, *ApJ*, 640, 308
- Marrone, D. P., Moran, J. M., Zhao, J.-H., & Rao, R. 2007, *ApJ*, 654, L57
- Mathur, S. D. 2007, in *Proceedings of the 4th Aegean Summer School on Black Holes, Mytilene (Greece)*, Vol. 803
- McClintock, J. E., Narayan, R., & Rybicki, G. B. 2004, *ApJ*, 615, 402
- Moneti, A. et al. 2001, *A&A*, 366, 106
- Narayan, R., Garcia, M. R., & McClintock, J. E. 1997, *ApJ*, 478, L79
- Narayan, R. & Heyl, J. S. 2002, *ApJ*, 574, L139
- Narayan, R. & McClintock, J. E. 2008, *New Astronomy Review*, 51, 733
- Narayan, R., Yi, I., & Mahadevan, R. 1995, *Nature*, 374, 623
- Oppenheimer, J. R. & Snyder, H. 1939, *Physical Review*, 56, 455
- Penrose, R. 1965, *Physical Review Letters*, 14, 57
- Quataert, E. & Gruzinov, A. 2000, *ApJ*, 545, 842
- Schödel, R. et al. 2007, *A&A*, 462, L1
- Shen, Z.-Q. et al. 2005, *Nature*, 438, 62
- Wheeler, J. A. 1966, *ARA&A*, 4, 393